Suppression of Phase Transitions in a Confined Rodlike Liquid Crystal

Christos Grigoriadis,[†] Hatice Duran,[§,⊥] Martin Steinhart,[¶] Michael Kappl,[§] Hans-Jürgen Butt,[§] and George Floudas[†,‡,*]

[†]Department of Physics, University of Ioannina, 451 10 Ioannina, Greece, [‡]Foundation for Research and Technology, Biomedical Research Institute, Ioannina, Greece, [§]Max Planck Institute for Polymer Research, Ackermannweg 10, 55128 Mainz, Germany, [⊥]TOBB University of Economics and Technology, Söğütözü Cad. 43, 06560 Ankara, Turkey, and [¶]Institut für Chemie, Universität Osnabrück, D-49069 Osnabrück, Germany

ABSTRACT The nematic-to-isotropic, crystal-to-nematic, and supercooled liquid-to-glass temperatures are studied in the liquid crystal 4-pentyl-4′-cyanobiphenyl (5CB) confined in self-ordered nanoporous alumina. The nematic-to-isotropic and the crystal-to-nematic transition temperatures are reduced linearly with the inverse pore diameter. The finding that the crystalline phase is completely suppressed in pores having diameters of 35 nm and below yields an estimate of the critical nucleus size. The liquid-to-glass temperature is reduced in confinement as anticipated by the model of rotational diffusion within a cavity. These results provide the pertinent phase diagram for a confined liquid crystal and are of technological relevance for the design of liquid crystal-based devices with tunable optical, thermal, and dielectric properties.

KEYWORDS: rodlike liquid crystals · confinement · phase transitions · template synthesis · nanoporous alumina

Understanding the physical properties of liquid crystals spatially confined to the mesoscopic scale is of fundamental and technological importance as a significant portion of liquid crystals in device components is located near hard confining interfaces.[1] Mesophase orientation induced by surface anchoring and wall-induced density modulations have length scales that compete with the length scales set by elasticity as well as by the bulk correlations.[2−7] Hence, the equilibrium director field morphology and final optical and dielectric properties of liquid crystal-based components depend on the elastic constants, surface coupling, the size of the system and its density as well as on applied external fields.

There are several important studies mainly with dielectric spectroscopy,[8−15] differential scanning calorimetry,[8,16] NMR,[6,7,17] and X-ray scattering,[18] on the molecular dynamics of different alkylcyanobiphenyls in porous membranes. The latter, however, lacked uniformity—both in length and diameter—that is necessary to address the above-mentioned issues. On the other hand, self-ordered nanoporous aluminum oxide (AAO)[19−22] has been widely used as an inorganic model matrix as it contains arrays of straight cylindrical nanopores, uniform in length and diameter, that can easily be infiltrated with liquid crystals or low viscosity polymeric melts.[23−25] It is already known that hard confinement imposed by the rigid AAO pore walls can suppress phase transitions. With respect to polymer crystallization, we have recently shown[25] a transformation from a predominantly heterogeneous to a predominantly homogeneous nucleation in isotactic polypropylene for pore sizes below 65 nm and a complete suppression of crystallization below 20 nm indicating the critical nucleus size.

In this work, we explore the effect of confinement on the thermodynamic stability of phases and on the molecular dynamics of the liquid crystal 4-pentyl-4′-cyanobiphenyl (5CB) within self-ordered AAO. In particular, we address how the nematic-to-isotropic (N/I) and crystal-to-nematic (C/N) phase transitions as well as the molecular mobility are affected by the confinement. We report a reduction and broadening of the transition temperatures and a complete suppression of the C/N phase transition in AAO pores with diameters of ∼35 nm and below. In addition, 5CB orientation dynamics is faster in confinement and possesses a broad distribution of relaxation times.

RESULTS AND DISCUSSION

Self-ordered AAO (pore diameters of 25, 35, 65, 180, and 380 nm; pore depth 80 to 100 μm) was prepared following the procedures reported in the literature.[9] Figure 1a shows a scanning electron microscopy (SEM) image of self-ordered AAO anodized with oxalic acid, Figure 1b shows a SEM image of commercially available disordered AAO filters (Whatman Anodisc) with a nominal pore diameter of 20 nm (which is the

* Address correspondence to gfloudas@cc.uoi.gr.

Received for review September 7, 2011 and accepted October 5, 2011.

Published online October 05, 2011 10.1021/nn203448c

© 2011 American Chemical Society

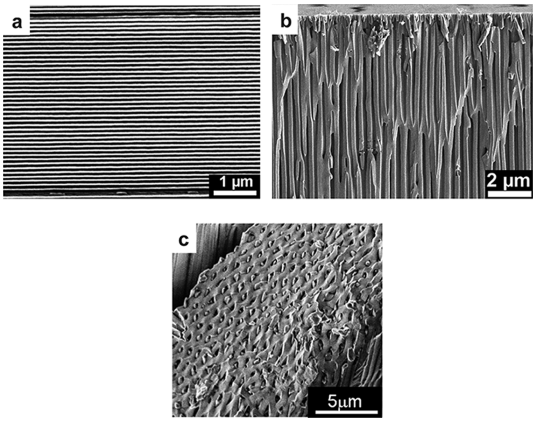

Figure 1. (a) Scanning electron microscopy image of self-ordered AAO anodized with oxalic acid prepared following procedures described elsewhere.[19] (b) SEM image of commercially available disordered AAO (Whatman Anodisc), nominal pore diameter 20 nm. Whatman Anodisc membranes are designed as filters having a thin size-selective layer (on the top) with narrow pores supported by a thick layer with larger pores having diameters scattering about 200 nm in order to reduce flow resistance in the course of separation processes. The pore size distributions are broad; the pores are partially interconnected. (c) Cryo-SEM image of an ODPA-modified AAO membrane having a pore diameter of 180 nm after infiltration with 5CB.

pore diameter of a thin size-selective layer on top of a thick support layer with pore diameters scattering about 200 nm). It can be clearly seen that only self-ordered AAO can be considered as uniform matrix imposing well-defined confinement on materials located in the pores. Infiltration of the 5CB was performed by placing neat 5CB on the surface of self-ordered AAO at 473 K for 20 h under vacuum or in argon atmosphere. Cryo-SEM investigations carried out at 93 K revealed that under the conditions applied the pores of the self-ordered AAO were completely filled with 5CB, even if the pore walls are modified with octadecylphosphonic acid (ODPA, see below) so that they are covered with a nonpolar alkyl layer (Figure 1c). Prior to any further use, excess 5CB was removed from the surface of the self-ordered AAO membranes.

Figure 2 displays the differential scanning calorimeter (DSC) thermograms of bulk 5CB and of the 5CB inside self-ordered AAO obtained on heating (rate 10 K/min). At 297.8 and 309.4 K the crystal-to-nematic (C/N) and nematic-to-isotropic (N/I) transitions with respective heats of 56.5 and 1.7 J/g are evident in bulk 5CB. Drastic changes occur when 5CB is located inside the pores of self-ordered AAO. First the N/I transition temperature apparently increases for pore diameters of 380 nm and then systematically decreases with decreasing pore diameter. The heat of fusion decreases to a fifth of the bulk value for 5CB in self-ordered AAO with a pore diameter of 25 nm. Second, the C/N transition broadens significantly and shifts to lower temperatures, whereas the crystalline phase is completely suppressed in pores with diameters of 35 nm and below.

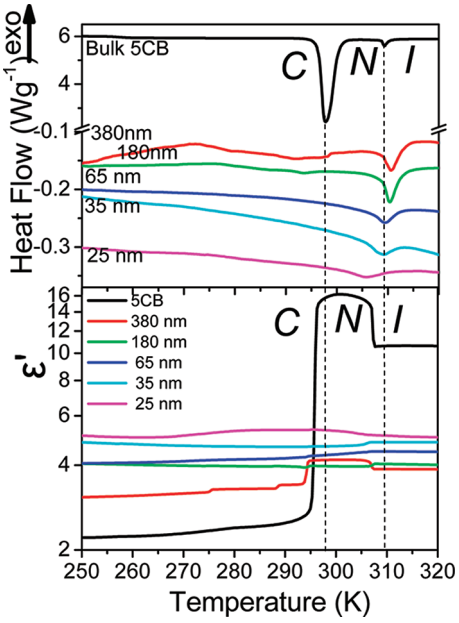

Figure 2. (Top) Thermograms of bulk 5CB and of 5CB located inside native self-ordered AAO with pore diameters ranging from 380 to 25 nm obtained at a heating rate of 10 K/min. The vertical dashed lines indicate the transition temperatures of bulk 5CB. (Bottom) Temperature dependence of the dielectric permittivity of the same samples at a frequency of 8×10^5 Hz. The vertical dashed lines indicate the transition temperatures of bulk 5CB from DSC. The letters C, N, and I stand for crystalline, nematic, and isotropic, respectively.

Dielectric spectroscopy (DS) is a versatile technique to probe the dynamics of rodlike molecules possessing a large dipole moment, such as 5CB. The complex dielectric permittivity $\varepsilon^* = \varepsilon' - i\varepsilon''$, where ε' is the real and ε'' is the imaginary part of the dielectric function, is generally a function of frequency ω and temperature T. Both the orientation polarization of permanent dipoles and conductivity contribute to ε^*. The orientational contribution can be fitted using the empirical equation of Havriliak and Negami. The temperature dependence of the ε' is a sensitive probe of the phase behavior and of the local packing of 5CB molecules. In addition, the derivative of the ε' with respect to temperature, $d\varepsilon'/dT$ is a very sensitive probe of the transition temperatures.[14,15] On heating from the low temperature C phase (Figure 2), ε' increases on entering the nematic phase because of the increased dynamics of the molecules possessing large dipoles. At the N/I transition the permittivity drops, signifying an increasing concentration of 5CB dimers with antiparallel dipole−dipole correlations.[26] The permittivity of the 5CB-infiltrated self-ordered AAO with pore diameter of 380 nm displays a similar dependence albeit with smaller steps at the respective transition temperature. In addition, two more steps at lower temperatures were observed (~275 and ~288 K). However, the temperature dependence of the permittivity of 5CB in self-ordered AAO with smaller pore diameters

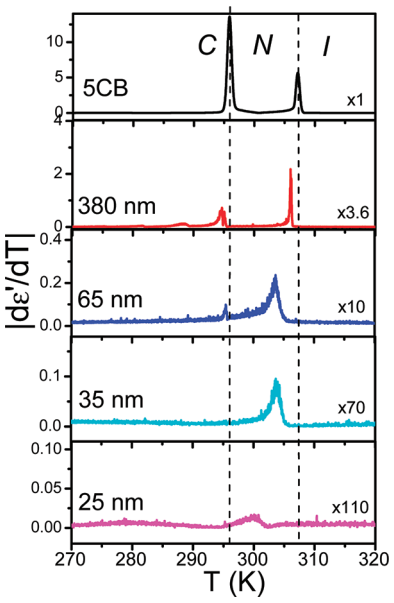

Figure 3. Absolute derivative of the dielectric permittivity as a function of temperature of bulk 5CB and of 5CB located inside ODPA-modified self-ordered AAO obtained at a heating rate of 1 K/min. The vertical axes were multiplied by appropriate factors as indicated. The vertical dashed lines indicate the transition temperatures of bulk 5CB.

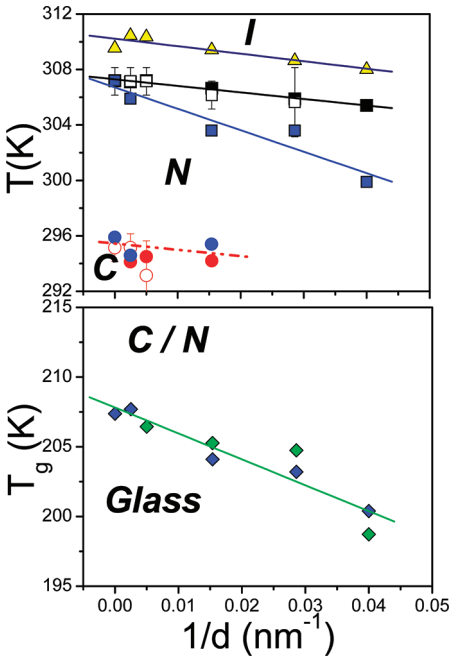

Figure 4. Dependence of the transition temperatures of bulk 5CB and of 5CB located inside self-ordered AAO plotted as a function of the inverse pore diameter 1/*d*. The symbols correspond to (top) (up filled triangles) nematic-to-isotropic (N/I) transition from DSC (rate 10 K/min); (filled black squares) nematic-to-isotropic transition from isochronal DS measurements; (open square) nematic-to-isotropic transition from isothermal DS measurements; (filled red spheres) crystal-to-nematic transition (C/N) from isochronal DS measurements; (open red circles) crystal-to-nematic transition from isothermal DS measurements; (blue filled squares) nematic-to-isotropic (N/I) transition in ODPA-modified AAO from isochronal DS measurements; (blue spheres) crystal-to-nematic transition in ODPA-modified AAO from isochronal DS measurements. (Bottom) liquid-to-glass temperature in native (green rhombi) and ODPA-modified (blue rhombi) AAO.

displayed significantly weaker features especially at the C/N transition. The N/I transition was still visible but the dielectric permittivity in the N phase was now lower than in the I phase, suggesting the presence of dimers with persistent antiparallel dipole correlations. The transition temperatures can best be extracted from the temperature dependence of the derivative of the dielectric permittivity with temperature (Supporting Information, Figure S1 and Figure 3, for the 5CB located inside native and ODPA treated AAO, respectively). In addition, the transition temperatures as well as the 5CB dynamics within the different phases can be extracted from the frequency-dependent dielectric loss spectra obtained for a range of temperatures. These data show a small but systematic reduction in both N/I and C/N transition temperatures upon confinement. A shift in the transition temperature can result from different competing effects: surface-induced ordering that may increase the transition temperature and a stronger disordering effect from the elastic forces that tend to reduce the transition temperature. In addition, both effects can lead to density modulations near the walls.

To explore the effect of surface anchoring, alkyl chains were grafted onto the AAO pore walls by modifying them with ODPA. ODPA adsorbed from organic solvents forms stable monolayers on amorphous alumina surfaces[27] so that hydrophobic low-energy surfaces result.[28] While the length of a fully extended ODPA molecule—the alkyl moiety of which adopts an all-*trans* conformation—amounts to 23.5 Å, the thickness of ODPA monolayers on crystalline alumina substrates was predicted to lie in the range from 18.1 Å to 23.6 Å. Thicknesses smaller than that of extended all-trans ODPA were ascribed to a tilted orientation of the ODPA molecules with respect to the substrate surface and to chain distortion.[29] Modification of AAO with ODPA influences the phase transitions of 5CB. This is well represented by plotting the temperature derivative of the dielectric permittivity, as seen in Figure 3, revealing systematic reduction in the N/I transition temperatures and the complete suppression of crystallization in pores with diameters of 35 nm and below. In addition, the sharp N/I transition in bulk 5CB and in ODPA-modified self-ordered AAO with a pore diameter of 380 nm broadens significantly for pore diameters below 65 nm and is barely detectable in the 25 nm pores. This observation is consistent with the theoretically predicted rounding of first order phase transitions upon confinement[2] and the reported difficulty in obtaining smectic phases of molecular rods that where homeotropically aligned at the confining walls.[30] At this point we should mention that for nanochannel-confined rodlike liquid crystals a true N/I transition may not exist.[31] The anchoring at

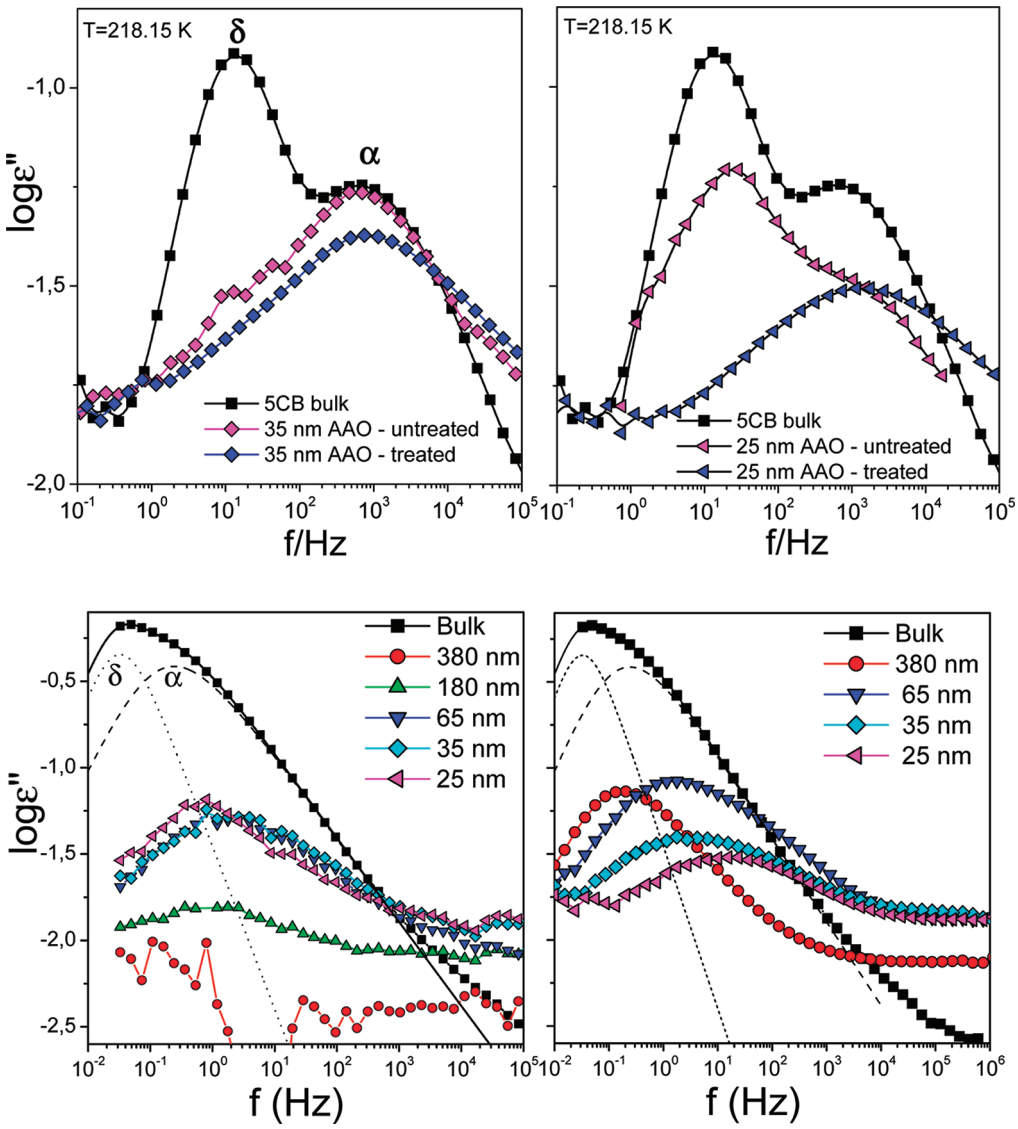

Figure 5. (Top) Dielectric loss spectra of bulk 5CB (squares) and of 5CB located inside self-ordered AAO with pore diameters of 35 nm (left) and 25 nm (right) and with native (magenta) and ODPA-modified (blue) pore walls shown at 218.15 K. Notice the suppression of the slow (δ) process within AAO having a pore diameter of 35 nm and the opposite effect within AAO having a pore diameter of 25 nm. (Bottom) Dielectric loss spectra of bulk 5CB (squares) and of 5CB located inside self-ordered AAO with native (left) and ODPA-modified (right) pore walls at 208.15 K for different pore diameters. Notice 5CB fully (partially) crystallizes within native pores with pore diameter of 380 (180) nm but not within the smaller pores. The dashed and dotted lines are Havriliak–Negami fits to the 5CB data.

the confining walls (*i.e.,* the surface field) can impose a partial nematic ordering even at temperatures above the bulk N/I transition. In addition, the symmetry breaking is not spontaneous, as expected for a genuine phase transition, but is enforced by the interactions with the walls.

The pore diameter dependence of the transition temperatures is summarized in Figure 4 both for the 5CB confined to native and ODPA-modified (blue symbols) self-ordered AAO. The reduction in both N/I and C/N transition temperatures with decreasing pore diameter is more pronounced in the case of the ODPA-modified self-ordered AAO. The DSC results on the N/I transition temperature for the 5CB in native AAO can be parametrized as $T_{N/I} = 310 - 55/d$, where d is the pore diameter and T the absolute temperature in K. This outcome is in agreement with the results obtained by DS ($T_{N/I} = 307.3 - 47/d$), despite a difference in the actual transition temperatures (reflecting the different rates of DSC and DS measurements). For the C/N transition a similar reduction in $T_{C/N}$ is obtained, although in this case the transition is completely suppressed for the smaller pores. In the case of the ODPA-modified self-ordered AAO the N/I transition temperature scales as $T_{N/I} = 306.7 - 155/d$, that is, a much stronger decrease is seen. This outcome may have two origins: first a surface phosphonate layer of ~2 nm reduces the effective pore diameter available to 5CB molecules especially in the smaller pores. However, a steeper dependence remains even if a

correspondingly smaller effective pore diameter is assumed. Second, it is reasonable to assume that 5CB and the ODPA alkyl moieties show high compatibility particularly mediated by the pentyl moiety of the 5CB.[16] Hence, an interphase consisting of the octadecyl moieties of ODPA and 5CB may exist, from which disorder and orientational defects propagate into 5CB located away from the pore walls. It is straightforward to assume that this effect is the more pronounced the smaller the AAO pore diameters are. As reported previously, specific heat measurements on confined 5CB indeed displayed an orientation-driven reduction in the transition temperature with a stronger suppression for the radial orientation.[16]

The geometrical frustration of molecular rods near the pore walls may lead to a decreasing density. In this view, we associate the pore diameter with pressure. Thus, increasing confinement can be as though being equivalent to decreasing pressure (*i.e.*, decreasing density). Pressure–volume–temperature measurements[32] of 5CB revealed a positive pressure coefficient for the N/I and C/N transitions with values of $dT_{N/I}/dP = 0.46$ K/MPa and $dT_{C/N}/dP = 0.284$ K/MPa, respectively. In this context, an ~2 K reduction in $T_{N/I}$ of 5CB residing in self-ordered AAO with small pore diameters can be associated with a decrease in pressure by 4.7 MPa that results in a reduction in density of 3×10^{-3} g/cm^3 (~0.3%) within the nematic phase. Similarly, a reduction in $T_{C/N}$ by 1.5 K in the smaller pores can be associated with a decrease in pressure of 5.3 MPa that results in a decrease in density of 1×10^{-3} g/cm^3. These results are reasonable estimates for the density within the nematic and crystalline phases of confined 5CB.[32] Interestingly, Figure 4 provides the pertinent phase diagram for a confined liquid crystal.

The density-driven effects on the phase transitions discussed above are accompanied by confinement-induced changes of the 5CB orientation dynamics. The dynamics of rodlike liquid crystals in the nematic phase reflect rotations about their long and short molecular axes.[33,34,8] These dynamic features give rise to fast (called α) and to hindered, that is, slow (called δ) processes that are very distinct within the nematic phase because the nematic potential hinders rotation about the short axis. The intensity of the two modes depends on the orientation of the director with respect to the external electric field. For example, a director aligned parallel (perpendicular) to the electric field favors relaxation through the slower (faster) process. Figure 5 shows representative dielectric loss spectra of bulk 5CB (squares) and of 5CB located inside self-ordered AAO as a function of the pore diameter. From the relative dielectric strength apparent in the dielectric loss spectra we can conclude that 5CB within native self-ordered AAO with a pore diameter of 35 nm has the director predominantly oriented perpendicular to the electric field (*planar radial*), whereas within self-ordered AAO with a pore diameter of 25 nm the director is predominantly oriented parallel to the electric field (*axial* or *escaped radial*). To our knowledge such a change of orientation has not been reported before (the reason could be the limited uniformity of the employed porous membranes). However, in agreement with experiment[8,12] and theory,[6,7] independent of the pore size the predominant orientation within surface-modified self-ordered AAO is planar radial. The theory predicts a structural transition driven by a homeotropic-to-planar anchoring transition in the nematic phase if the pore walls are modified with coupling agents having linear alkyl moieties with more than seven carbon atoms as a result of steric interactions. In addition, all spectra modes display broader relaxation spectra in confinement.

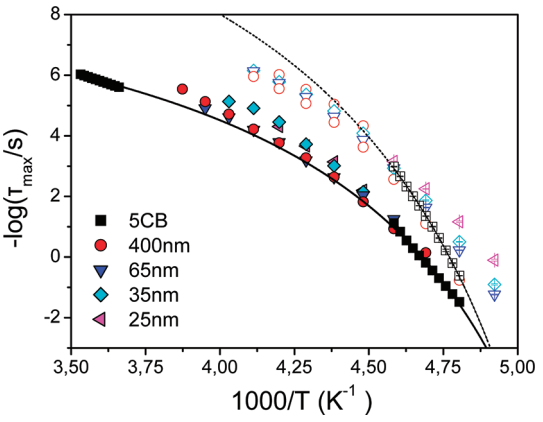

Figure 6. Relaxation times of the fast (open symbols) and slow (filled symbols) dynamics of 5CB in the bulk (squares) and of 5CB located inside ODPA-modified self-ordered AAO with diameters from 400 to 25 nm. The solid and dashed lines are VFT fits to the slow (δ) and fast (α) processes in bulk 5CB times.

Independent of the dielectric strength, both the α process and the δ process obey the Vogel–Fulcher–Tammann (VFT) equation, $\tau = \tau_0 \exp(B/T - T_0)$, where τ_0 is the relaxation time in the limit of very high temperatures, B is the activation parameter, and T_0 is the "ideal" glass temperature located below the glass temperature T_g.[35] Figure 6 displays the relaxation times at maximum loss corresponding to bulk 5CB and for 5CB located inside ODPA-modified self-ordered AAO. For bulk 5CB the δ process—being well within the experimental window—can be followed by cooling from higher temperatures down to ~273 K. At this temperature, crystallization sets in that freezes the molecular dynamics and diminishes the dielectric strength. To follow the 5CB dynamics to even lower temperatures the sample was quenched from the nematic phase with liquid nitrogen to 77 K. Subsequently, isothermal frequency sweeps were made on heating up to 218 K, a temperature above which the rate of crystallization is too high. On the other hand, the crystallization of 5CB located inside ODPA-modified self-ordered AAO is suppressed (Figure 3 and Figure 5) and the dynamics corresponding to the α

process and the δ processes can easily be followed to lower temperatures in the vicinity of T_g.

The extracted glass temperatures (defined as the temperature where the α process relaxation time is at ~10 s) are also plotted in Figure 4 for bulk 5CB and for 5CB located inside ODPA-modified self-ordered AAO with different pore diameters. The glass temperature of 5CB is reduced in confinement according to $T_g = 207.8 - 185/d$ for both ODPA-modified and native self-ordered AAO. The enhanced mobility within the pores can be understood by considering the model of a molecular rod relaxing within a cavity.[36] According to the rotational diffusion model, a molecule with cylindrical symmetry possessing a dipole moment along the symmetry axis will rotate faster when confined within a conical volume. Thus, the observed acceleration of rotation (at $T = 210$ K) in confinement by factors of 2.4, 5.9, 7.6, and 45 as compared to the bulk relaxation time for 5CB residing in self-ordered AAO with pore diameters of 180, 65, 35, and 25 nm reflects increasing confinement with respective cone angles of 46°, 31°, 26°, and 12°.

CONCLUSIONS

In summary, the cylindrical confinement imposed by self-ordered nanoporous alumina affects both thermodynamic phase transitions and molecular dynamics of the rodlike liquid crystal 5CB. The investigation of the pore-size dependence of transition temperatures allowed the construction of the pertinent phase diagram for a confined liquid crystal. The nematic-to-isotropic and the crystal-to-nematic transition temperatures are reduced and scale linearly with d^{-1}. Furthermore, the crystalline phase is completely suppressed in AAO with pores having diameters of 35 nm and below, a finding that allows estimating the critical nucleus size. The glass transition temperature is also reduced. Increasing the degree of confinement by reducing the pore diameter is accompanied by faster orientational dynamics of 5CB, as anticipated by the model of rotational diffusion within a cavity. These results are of technological relevance for the design of LC-based components with tunable optical, thermal, and dielectric properties.

METHODS

Sample Preparation and Characterization. The investigated liquid crystal was 4-pentyl-4′-cyanobiphenyl, known as 5CB (Synthon AcMaRi Chemie GmbH). Self-ordered nanoporous alumina templates (pore diameters: 25, 35, 65, 180, and 380 nm; pore depth between 80 and 100 μm) were prepared following the procedures reported in the literature.[19−21] Prior to further use, all AAO membranes were heated to 200 °C overnight under vacuum.

Infiltration of 5CB into Nanoporous Alumina. Prior to infiltration with 5CB, empty AAO membranes were weighed using a microbalance (Mettler-Toledo, MX5) with an accuracy of 1 ± 0.8 μg at least for three times. Then, the liquid crystal 5CB was spread on native AAO or AAO surface-modified with ODPA at 330 K (T_{NI} + 20 K) until the entire AAO membrane was covered with liquid 5CB. The 5CB-loaded AAO membranes were kept under a vacuum of 200 mbar for 8 h at a temperature of 325 K. Then, the samples were quenched with liquid nitrogen, and residual 5CB was removed from the AAO surfaces with sharp razor blades and soft polishing paper (Buehler Microcloth). Then, the infiltrated AAO membranes were again weighed. The weight difference between infiltrated AAO and empty AAO was assumed to correspond to the mass of the infiltrated 5CB.

Monitoring the Thermal Behavior. Thermal analyses were carried out with a Mettler Toledo Star DSC. A 3−5 mg portion of the sample material was placed in aluminum pans that were sealed before the measurements. In the case of neat 5CB, empty aluminum pans were used as reference while in the case of AAO infiltrated with 5CB native AAO membrane pieces with the same pore diameter, the same pore depth, and the same area were used as reference samples. The samples were first cooled at a rate of 10 K/min from ambient temperature to 173 K and then heated to 333 K at the same rate in a nitrogen atmosphere. The same cycle was repeated two times and the results from the second heating and cooling thermographs were employed in the analysis of the phase transition (isotropic, nematic, and crystalline) temperatures.

Surface Modification with ODPA. Octadecylphosphonic acid ($C_{18}H_{39}O_3P$; ODPA) was purchased from Alfa Aesar. Self-ordered AAO was activated in 30% aqueous H_2O_2 solution for 2 h at 45 °C, dried at 120 °C for 15 min, and immersed for 48 h at 25 °C into a 4.2 mM solution of ODPA in a *n*-heptane/isopropyl alcohol (v:v/5:1) solvent mixture. Subsequently, the substrates were washed with copious amounts of *n*-heptane/isopropyl alcohol and sonicated to remove any physisorbed (not grafted) ODPA. Subsequently, the ODPA-modified AAO was washed with heptane/isopropyl alcohol mixtures as well as with acetone for several times and then dried overnight under vacuum (200 mbar) at room temperature.

Cryo-SEM. Low-temperature SEM images were acquired with a FEI Nova600 NanoLab Dualbeam SEM/focused ion beam (FIB) system equipped with a cryogenic preparation chamber (Quorum Technologies) using a "through the lens" secondary electron detector. 5CB-filled AAO membranes were sectioned with focused ion beams inside the cryo-preparation chamber under a vacuum of 2×10^{-5} mbar vacuum at 93 K and then imaged under cryoscopic conditions at an acceleration voltage of 2 kV.

Dielectric Spectroscopy (DS). The dielectric measurements were performed at different temperatures in the range of 123−473 K, at atmospheric pressure, and for frequencies in the range from 10^{-2} to 10^6 Hz using a Novocontrol BDS system composed of a frequency response analyzer (Solartron Schlumberger FRA 1260), a broadband dielectric converter and an active sample hand. For bulk 5CB, the DS measurements were carried out in the usual parallel plate geometry with electrodes of 20 mm in diameter and a sample thickness of 50 μm maintained by Teflon spacers. For the 5CB infiltrated self-ordered AAO we used samples as those shown in Figure 1a. In this case, the sample cell consisted of two parallel plate electrodes 20 mm in diameter with the AAO pore axes oriented perpendicular to the electrodes. The sample thickness corresponded to the pore length (~80 μm). The measured dielectric spectra were corrected for the geometry as follows: two capacitors in parallel composed of ε^*_{5CB} and ε^*_{AAO} were employed and the measured total impedance was related to the individual values through $1/Z^*_{total} = 1/Z^*_{5CB} + 1/Z^*_{AAO}$. This allowed calculating the real and imaginary parts of the dielectric permittivity as a function of the respective volume fractions as

$$\varepsilon'_{5CB} = \frac{\varepsilon'_{total} - \varphi_{AAO}\varepsilon'_{AAO}}{\varphi_{5CB}} \qquad (1)$$

$$\varepsilon''_{5CB} = \frac{\varepsilon''_{total}}{\varphi_{5CB}}$$

The latter were obtained by digitization of the SEM images. There are two principal mechanisms that contribute to ε^* in our case: orientation polarization of permanent dipoles (ε^*_{dip}) and conductivity contributions (ε^*_{cond}) as: $\varepsilon^*(\omega, T, P) = \varepsilon^*_{dip}(\omega, T, P) - i\sigma(T,P)/(\varepsilon_f\omega)$ where σ is the dc conductivity and ε_f is the permittivity of free space. The orientational contribution was fitted using the Havriliak−Negami equation

$$\varepsilon^*_{dip}(\omega, T, P) = \varepsilon_\infty(T, P) + \sum_{k=1}^{2} \frac{\Delta\varepsilon_k(T, P)}{[1 + (i\omega\tau_{HN}(T, P)^{m_k}]^{n_k}} \quad (2)$$

where $\Delta\varepsilon_k(T,P)$ is the relaxation strength of the process under investigation, τ_{HN} is the relaxation time, m and n ($0 < m; mn \leq 1$) describe the symmetrical and asymmetrical broadening of the distribution of relaxation times, and $\varepsilon_\infty(T,P)$ is the dielectric permittivity at the limit of high frequencies. The relaxation times at maximum loss (τ_{max}) are presented herein and have been analytically obtained from the Havriliak−Negami equation as follows:

$$\left[\sin\left(\frac{\pi m}{2+2n}\right)\right]^{1/m} \tau_{max} = \tau_{HN}\left[\sin\left(\frac{\pi mn}{2+2n}\right)\right]^{1/m} \quad (3)$$

Acknowledgment. The current work was supported by the Research unit on Dynamics and Thermodynamics of the UoI cofinanced by the European Union and the Greek state under NSRF 2007-2013 (Region of Epirus, call 18). The authors thank C. Schröper and H. Tobergte for the preparation of AAO membranes, M. Mueller for Cryo-SEM measurements, and G. Tsoumanis for technical support (UoI). H.D. and M.S. gratefully acknowledge financial support from the German Research Foundation (SPP 1369 and STE 1127/14).

Supporting Information Available: Temperature dependence of the derivative of the dielectric permittivity of bulk 5CB and of 5CB located inside native self-ordered AAO. This material is available free of charge *via* the Internet at http://pubs.acs.org.

REFERENCES AND NOTES

1. Crawford, G. P., Zumer, S., Eds. *Liquid Crystals in Complex Geometries*; Taylor and Francis: London, 1996.
2. Wilms, D.; Winkler, A.; Virnau, P.; Binder, K. Rounding of Phase Transitions in Cylindrical Pores. *Phys. Rev. Lett.* **2010**, *105*, 045701.
3. van der Beek, D.; Reich, H.; van der Schoot, P.; Dijkstra, M.; Schilling, T.; Vink, R.; Schmidt, M.; van Roij, R.; Lekkerkerker, H. Isotropic-Nematic Interface and Wetting in Suspensions of Colloidal Platelets. *Phys. Rev. Lett.* **2006**, *97*, 087801.
4. Trukhina, Y.; Schilling, T. Computer Simulation Study of a Liquid Crystal Confined to a Spherical Cavity. *Phys. Rev. E* **2008**, *77*, 011701.
5. Schilling, T.; Frenkel, D. Self-Poisoning of Crystal Nuclei in Hard-Rod Liquids. *Phys. Rev. Lett.* **2004**, *92*, 085505.
6. Crawford, G. P.; Allender, D. W.; Doane, J. W. Surface Elastic and Molecular-Anchoring Properties of Nematic Liquid-Crystals Confined to Cylindrical Cavities. *Phys. Rev. A* **1992**, *45*, 8693–8708.
7. Crawford, G. P.; Ondriscrawford, R.; Zumer, S.; Doane, J. W. Anchoring and Orientational Wetting Transitions of Confined Liquid-Crystals. *Phys. Rev. Lett.* **1993**, *70*, 1838–1841.
8. Rozanski, S. A.; Stannarius, R.; Groothues, H.; Kremer, F. Dielectric Properties of the Nematic Liquid Crystal 4-*n*-Pentyl-4′-cyanobiphenyl in Porous Membranes. *Liq. Cryst.* **1996**, *20*, 59–66.
9. Sinha, G.; Leys, J.; Glorieux, C.; Thoen, J. Dielectric Spectroscopy of Aerosil-Dispersed Liquid Crystal Embedded in Anopore Membranes. *Phys. Rev. E* **2005**, *72*, 051710.
10. Sinha, G. P.; Aliev, F. M. Dielectric Spectroscopy of Liquid Crystals in Smectic, Nematic, and Isotropic Phases Confined in Random Porous Media. *Phys. Rev. E* **1998**, *58*, 2001–2010.
11. Schönhals, A.; Frunza, S.; Frunza, L.; Unruh, T.; Frick, B.; Zorn, R. Vibrational and Molecular Dynamics of a Nanoconfined Liquid Crystal. *Eur. Phys. J. Special Top.* **2010**, *189*, 251–255.
12. Bras, A. R.; Dionisio, M.; Schönhals, A. Confinement and Surface Effects on the Molecular Dynamics of a Nematic Mixture Investigated by Dielectric Relaxation Spectroscopy. *J. Phys. Chem. B* **2008**, *112*, 8227–8325.
13. Frunza, S.; Frunza, L.; Goerning, H.; Sturm, H.; Schönhals, A. On the Dynamics of Surface Layer in Noctalcyanobiphenyl-Aerosil Systems. *Europhys. Lett.* **2001**, *56*, 801.
14. Diez-Berart, S.; Lopez, D. O.; de la Fuente, M. R.; Salud, J.; Perez-Jubindo, M. A.; Finotello, D. Critical Behaviour in Liquid-Crystalline Phase Transitions: A Comparative Study of 9OCB in Bulk and Anopore Membranes. *Liq. Cryst.* **2010**, *37*, 893–901.
15. Lopez, D. O.; Perez-Jubindo, M. A.; de la Fuente, M. R.; Diez-Berart, S.; Salud, J. Influence of Cylindrical Submicrometer Confinement on the Static and Dynamic Properties in Nonyloxycyanobiphenyl (90CB). *J. Phys. Chem. B* **2008**, *112*, 6567–6577.
16. Iannacchione, G. S.; Finotello, D. Calorimetric Study of Phase-Transitions in Confined Liquid-Crystals. *Phys. Rev. Lett.* **1992**, *69*, 2094–2097.
17. Zidansek, A.; Lahajnar, G.; Kralj, S. Phase Transitions in 8CB Liquid Crystal Confined to a Controlled-Pore Glass: Deuteron NMR and Small Angle X-ray Scattering Studies. *Appl. Magn. Reson.* **2004**, *27*, 311–319.
18. Guegan, R.; Morineau, D.; Lefort, R.; Beziel, W.; Guendouz, M.; Noirez, L.; Henschel, A.; Huber, P. Rich Polymorphism of a Rodlike Liquid Crystal (8CB) Confined in Two Types of Unidirectional Nanopores. *Eur. Phys. J. E* **2008**, *26*, 261–273.
19. Masuda, H.; Fukuda, K. Ordered Metal Nanohole Arrays Made by a 2-Step Replication of Honeycomb Structures of Anodic Alumina. *Science* **1995**, *268*, 1466–1468.
20. Masuda, H.; Hasegwa, F.; Ono, S. Self-Ordering of Cell Arrangement of Anodic Porous Alumina Formed in Sulfuric Acid Solution. *J. Electrochem. Soc.* **1997**, *144*, L127–L130.
21. Masuda, H.; Yada, K.; Osaka, A. Self-Ordering of Cell Configuration of Anodic Porous Alumina with Large-Size Pores in Phosphoric Acid Solution. *Jpn. J. Appl. Phys. 2* **1998**, *37*, L1340–L1342.
22. Nielsch, K.; Choi, J.; Schwirn, K.; Wehrspohn, R. B.; Gosele, U. Self-Ordering Regimes of Porous Alumina: The 10% Porosity Rule. *Nano Lett.* **2002**, *2*, 677–680.
23. Steinhart, M. Supramolecular Organization of Polymeric Materials in Nanoporous Hard Templates. *Adv. Polym. Sci.* **2008**, *220*, 123–187.
24. Duran, H.; Gitsas, A.; Floudas, G.; Mondeshki, M.; Steinhart, M.; Knoll, W. Poly(γ-benzyl-L-glutamate) Peptides Confined to Nanoporous Alumina: Pore Diameter Dependence of Self-Assembly and Segmental Dynamics. *Macromolecules* **2009**, *42*, 2881–2885.
25. Duran, H.; Steinhart, M.; Butt, H. J.; Floudas, G. From Heterogeneous to Homogeneous Nucleation of Isotactic Poly(propylene) Confined to Nanoporous Alumina. *Nano Lett* **2011**, *11*, 1671–1675.
26. Kreul, H. G.; Urban, S.; Wurflinger, A. Dielectric Studies of Liquid-Crystals under High-Pressure—Static Permittivity and Dielectric-Relaxation in the Nematic Phase of Pentylcyanobiphenyl (5cb). *Phys. Rev. A* **1992**, *45*, 8624–8631.
27. Thissen, P.; Valtiner, M.; Grundmeier, G. Stability of Phosphonic Acid Self-Assembled Monolayers on Amorphous and Single-Crystalline Aluminum Oxide Surfaces in Aqueous Solution. *Langmuir* **2010**, *26*, 156–164.
28. Hoque, E.; DeRose, J. A.; Kulik, G.; Hoffmann, P.; Mathieu, H. J.; Bhushan, B. Alkylphosphonate Modified Aluminum Oxide Surfaces. *J. Phys. Chem. B* **2006**, *110*, 10855–10861.
29. Luschtinetz, R.; Oliveira, A. F.; Duarte, H. A.; Seifert, G. *Z. Anorg. Allg. Chem.* **2010**, 1506–1512.
30. Malijevsky, A.; Varga, S. Phase Behaviour of Parallel Hard Rods in Confinement: An Onsager Theory Study. *J. Phys. Condens. Mater.* **2010**, *22*, 076004.
31. Kityk, A. V.; Wolff, M.; Knorr, K.; Morineau, D.; Lefort, R.; Huber, P. Continuous Paranematic-to-Nematic Ordering Transitions of Liquid Crystals in Tubular Silica Nanochannels. *Phys. Rev. Lett.* **2008**, *101*, 187801.

32. Sandmann, M.; Busing, D.; Bruckert, T.; Wurflinger, A.; Urban, S.; Gestblom, B. PVT and Dielectric Measurements on 4-*n*-Pentyl-4′-cyano-biphenyl (5CB) under High Pressure. *Proc. SPIE.* **1998**, *3318*, 223–227.
33. Attard, G. S.; Araki, K.; Moura-Ramos, J. J.; Williams, G. Molecular-Dynamics and Macroscopic Alignment Properties of Thermotropic Liquid-Crystalline Side-Chain Polymers as Studied by Dielectric-Relaxation Spectroscopy. *Liq. Cryst.* **1988**, *3*, 861–879.
34. Bras, A. R.; Dionisio, M.; Huth, H.; Schick, Cr.; Schönhals, A. Origin of Glassy Dynamics in a Liquid Crystal Studied by Broadband Dielectric and Specific Heat Spectroscopy. *Phys. Rev. E* **2007**, *75*, 061708.
35. Zeller, H. R. Dielectric Relaxation and the Glass Transition in Nematic Liquid Crystals. *Phys. Rev. Lett.* **1982**, *48*, 334–337.
36. Wang, C. C.; Pecora, R. Time-Correlation Functions for Restricted Rotational Diffusion. *J. Chem. Phys.* **1980**, *72*, 5333–5340.